Journal of Alloys and Compounds 509 (2011) 6689–6695

Contents lists available at ScienceDirect

Journal of Alloys and Compounds

journal homepage: www.elsevier.com/locate/jallcom

Fabrication of $ZnWO_4$ nanofibers by a high direct voltage electrospinning process

Yanee Keereeta [a], Titipun Thongtem [b,c,*], Somchai Thongtem [a,c]

[a] Department of Physics and Materials Science, Faculty of Science, Chiang Mai University, Chiang Mai 50200, Thailand
[b] Department of Chemistry, Faculty of Science, Chiang Mai University, Chiang Mai 50200, Thailand
[c] Materials Science Research Center, Faculty of Science, Chiang Mai University, Chiang Mai 50200, Thailand

ARTICLE INFO

Article history:
Received 25 February 2011
Received in revised form 21 March 2011
Accepted 24 March 2011
Available online 31 March 2011

Keywords:
Semiconductors
Nanofabrications
Luminescence
Scanning electron microscopy
X-ray diffraction

ABSTRACT

Mixtures of zinc acetate dihydrate, ammonium metatungstate hydrate, and 5 wt%, 6 wt%, and 7 wt% of poly (vinyl alcohol) (PVA) were electrospun by a +15 kV direct voltage to produce fibers. In the present research, the electrospun fibers of 6 wt% PVA were further calcined at 400–600 °C for 3 h. The sanmartinite monoclinic structured $ZnWO_4$ was detected by X-ray diffractometer (XRD) and selected area electron diffraction (SAED), weight loss by thermogravimetric analyser (TGA), morphology and particle size by scanning and transmission electron microscopes (SEM, TEM) and atomic force microscope (AFM), including their vibration modes by Fourier transform infrared spectrometer (FTIR) and Raman spectrometer. The 4.42 eV direct energy gap (E_g) and 460 nm emission wavelength, caused by the electronic transition of $(WO_6)^{2-}$ octahedrons, were determined by UV–visible absorption and photoluminescence (PL) spectrometers. A possible formation mechanism of $ZnWO_4$ nanofibers was also proposed according to the experimental results.

1. Introduction

Recently, nanostructured materials such as nanowires, nanorods, nanotubes and nanofibers have received considerable attention for a variety of applications [1]; especially, nanofibers or non-woven textiles [2]. They have attractive properties and novel potential applications for using as solar cells, electromagnetic shielding materials, non-wetting textiles, medical prosthesis, and liquid crystal devices [3,4]. A possible process used to produce nanofibrous inorganic materials is by electrospinning, which is now becoming increasingly popular [5] even for the industrial scale production. It is able to produce continuous polymer fibers with diameters of micro- and nano-scale through the action of an external electric field imposed in a polymer solution or melt [2]. By using the inorganic material and polymer mixtures as the starting precursors, the inorganic material–polymer electrospun fibers can be produced easily. When diameters of the electrospun fibers are lessened from micrometers to sub-micrometers or nanometers, there appear some amazing characteristics such as very large surface area to volume ratio, flexibility in surface functionality, and superior mechanical performance [4]. Subsequently, inorganic nanofibers can be produced by the calcination of inorganic material–polymer electrospun fibers obtained by electrospinning of the sol–gel solution [6].

Among different semiconducting materials, $ZnWO_4$ has excellent properties and strong potential application in various fields such as photoluminescence [7–9], Raman laser converters [7], photocatalyst [7], and scintillator material [7,10]. $ZnWO_4$ belongs to the monoclinic sanmartinite-type structure with $P2/c$ space group [11]. In the past decade, nanosized $ZnWO_4$ has been produced by several processes such as co-precipitation [7], Czochralski technique [12], hydrothermal method [8,13–15], microwave-assisted synthesis [16], and polymerized complex method [17].

To produce non-woven fibers by the electrospinning process, a positive high direct voltage is applied to a liquid droplet, ejected out of the tip of a hollow needle. The droplet is charged and stretched – known as Taylor cone. If the molecular cohesion of the liquid – such as polymeric solution or melt, and the direct voltage are sufficiently high, a very long thin charged liquid jet will be formed. During flying, the jet dries and solidifies – caused by the external electric field inside. Finally, the fiber is produced, and deposited on a grounded collector [4].

In the present research, $ZnWO_4$–PVA electrospun fibers were firstly produced by the lab-made electrospinning equipment. They are very novel and promising material for a variety of applications. These electrospun fibers were subsequently calcined at high temperature to form $ZnWO_4$ nanofibers. To the best of our knowledge, there are no $ZnWO_4$ nanofibers have ever been produced by the present process. It is therefore for us to use the mixture of inorganic materials and polymer to produce the inorganic material–polymer

* Corresponding author at: Department of Chemistry, Faculty of Science, Chiang Mai University, Chiang Mai 50200, Thailand. Tel.: +66 0 53 943344; fax: +66 0 53 892277.
E-mail address: ttpthongtem@yahoo.com (T. Thongtem).

0925-8388/$ – see front matter © 2011 Elsevier B.V. All rights reserved.
doi:10.1016/j.jallcom.2011.03.140

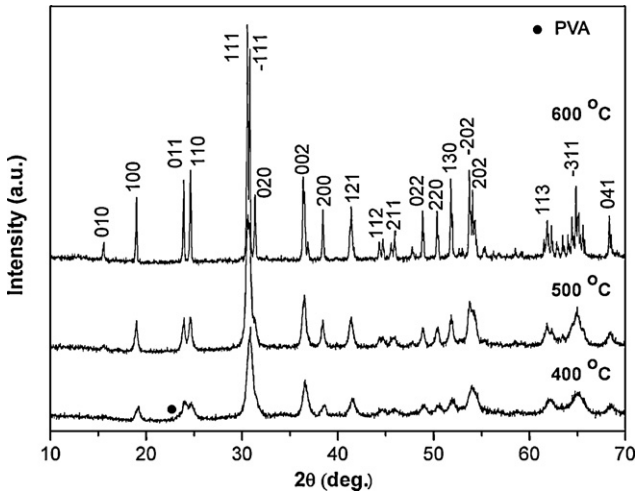

Fig. 1. XRD patterns of the electrospun fibers after calcination at 400 °C, 500 °C, and 600 °C for 3 h.

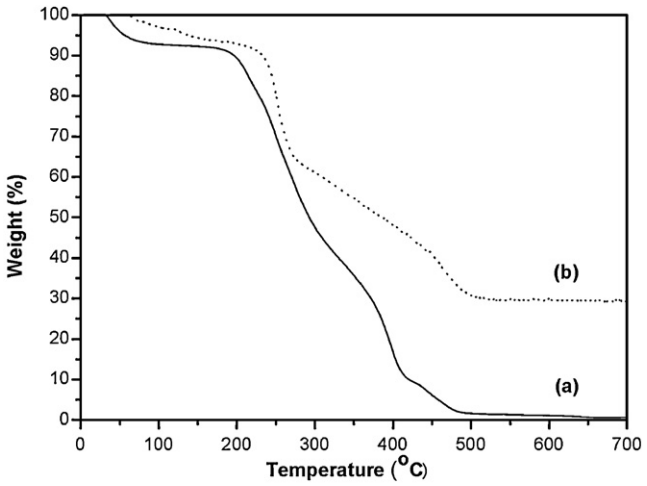

Fig. 2. TGA curves of (a) PVA, and (b) $ZnWO_4$–PVA electrospun fibers produced from 6 wt% PVA solution.

electrospun fibers, which would transform into nanofibrous inorganic material by subsequent calcination at high temperature. Moreover, the success in producing the solid nanofibrous material may lead to new industrial process under the action of an external electric field.

2. Experimental procedure

Basing on the conventional sol–gel process – 1:1 molar ratio of Zn:W of zinc acetate dihydrate ($Zn(CH_3COO)_2{\cdot}2H_2O$, 99.0%) and ammonium metatungstate hydrate ($H_{26}N_6O_{40}W_{12}{\cdot}H_2O$, 99.0%) was dissolved in 10 ml deionized water, and stirred for 10 min. Then 20 ml aqueous solutions of 5 wt%, 6 wt%, and 7 wt% poly (vinyl alcohol) (PVA, 125,000 MW) were added to the precursor solutions, with 30 min vigorous stirring in a 80 °C water bath. Each of the solution mixtures was loaded into a plastic syringe on a horizontal platform. A piece of flat aluminum foil was vertically placed 15 cm away for collecting the fibers. Electrospinning was done by ejecting a jet of inorganic material–polymeric solution out of the long hollow needle, and a +15 kV of d.c. power supply was simultaneously applied at the needle tip. Finally a dense web of electrospun fibers was collected on the grounded aluminum foil. The fibers produced from 6 wt% PVA solution was calcined by increasing from room temperature (T_R) at a rate of 5 °C/min until reaching 400 °C, 500 °C, and 600 °C, held at each of these temperatures for 3 h, and left the system to cool down to room temperature. The products were characterized using thermogravimetric analyser (TGA, Shimadzu TGA-50 analyzer, Japan) using a heating rate of 5 °C/min; X-ray diffractometer (XRD, SIEMENS D500, Germany) operating at 20 kV, 15 mA, and using Cu-Kα line, in combination with the database of the Joint Committee on Powder Diffraction Standards (JCPDS) [11]; scanning electron microscope (SEM, JEOL JSM-6335F, Japan) operating at 15 kV; transmission electron microscope (TEM, JEOL JEM-2010, Japan), high resolution transmission electron microscope (HRTEM) and selected area electron diffractometer (SAED) operating at 200 kV; atomic force microscope (AFM, NanoScope IIIa, MMAFML N, Veeco, USA) with silicon tip driven at a frequency of 200–300 kHz tapping mode; Fourier transform infrared spectrometer (FTIR, Bruker Tensor 27, Germany) with KBr as a diluting agent and operated in the range of 4000–400 cm^{-1}; Raman spectrometer (T64000 HORIBA Jobin Yvon, USA) using a 50 mW and 514.5 nm wavelength Ar green laser; UV–visible spectrometer (Lambda 25 PerkinElmer, USA) using a UV lamp with the resolution of 1 nm; and photoluminescence (PL) spectrometer (LS 50B PerkinElmer, USA) using a 280 nm excitation wavelength at room temperature.

3. Results and discussion

3.1. XRD

XRD patterns of the electrospun fibers after calcination at 400 °C, 500 °C and 600 °C are presented in Fig. 1. Comparing to the JCPDS database no. 15-0774 [11], they corresponded to sanmartinite structured $ZnWO_4$ with monoclinic crystal system and $P2/c$ space group. In the present study, temperature was found to have influence on the crystallinity and purity of $ZnWO_4$ fibers; especially, the relatively high temperature calcination. At 400 °C, XRD revealed that the product was not perfectly pure $ZnWO_4$. It contained some residual PVA at 2θ of approximately 22.5° [18]. Upon increasing the calcination temperatures to be 500 °C and 600 °C, the spectra became sharper and the XRD intensities were stronger. The crystalline degree of the products was much improved. No PVA was detected by the XRD. At 600 °C calcination, the product was the best pure crystal. Its degree of crystallinity was the highest, and the atoms resided in the perfect crystal lattice. By using the Scherrer formula [19], the crystallite sizes obtained by 400 °C, 500 °C, and 600 °C calcination for 3 h were 16 nm, 30 nm, and 105 nm, respectively.

3.2. TGA

Fig. 2 shows the thermal behavior of PVA and $ZnWO_4$–PVA electrospun fibers characterized by TGA analyzer with a heating rate of 5 °C/min. The weight loss of pure PVA exhibited the degradation process as follows. The first weight loss was 10.5%, due to the evaporation of loosely bound water at 32–200 °C. The second was the large amount of weight loss for 79.3%, predominantly caused by the decomposition of PVA structure at 200–420 °C. The third was 8.3%, by the breaking of PVA backbone at 420–490 °C. The weight loss tended to terminate upon further heating to above 490 °C [20]. When the $ZnWO_4$–PVA electrospun fibers were characterized, their weight losses were divided into three different steps. The first weight loss in the temperature range of 32–226 °C was 11.2%, and associated with water evaporation. The second weight loss of 45.7% at 226–420 °C was caused by the decomposition of PVA. The final weight loss of 15.5% in the temperature range of 420–519 °C was likely to be the oxidation and decomposition of the PVA main chain. These last two steps were attributed to the loss of PVA and organic compound blended in the fibers. At a temperature above 519 °C, there was no significant change in their weight. Thus, pure crystalline $ZnWO_4$ fibers were assumed to be produced at a temperature of 519 °C and above, very close to the reports of Zhao et al. (486 °C) [10], and Ryu et al. (550 °C) [17]. Comparing between PVA and $ZnWO_4$–PVA electrospun fibers, their weight and weight loss percents of each steps were different, mainly caused by the evaporation and decomposition of water and PVA.

3.3. SEM, TEM, AFM, and SAED

Fig. 3a–c shows SEM images of the electrospun fibers produced from the solutions of 5 wt%, 6 wt% and 7 wt% PVA. These products were composed of fibers shaped like a web of spiders,

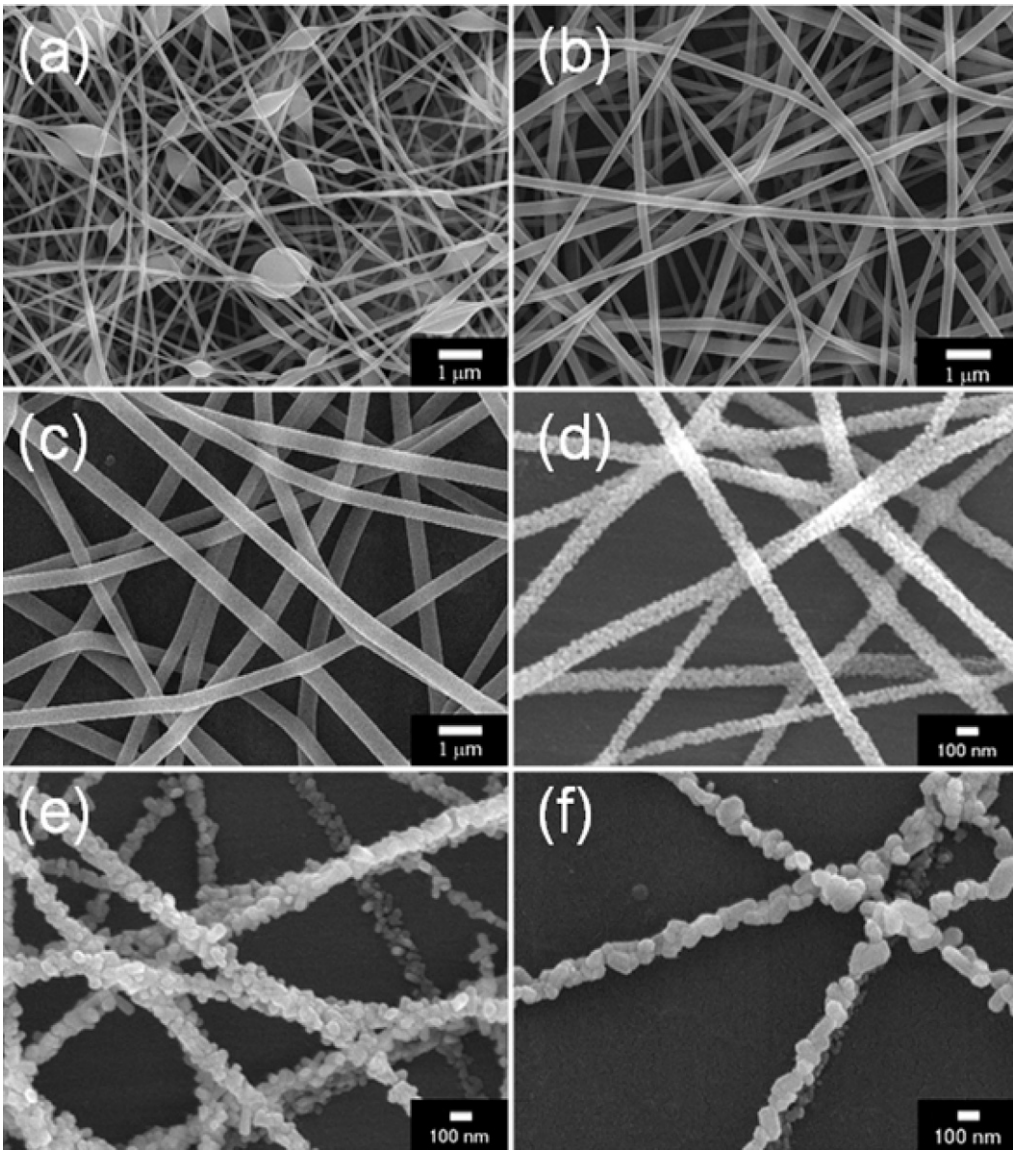

Fig. 3. SEM images of the electrospun fibers using different PVA contents of (a–c) 5 wt%, 6 wt%, and 7 wt%, and (d–f) the electrospun fibers of (b) after calcination at 400 °C, 500 °C, and 600 °C for 3 h, respectively.

with their smooth surfaces. The as-electrospun nuclei blended in the fibers were not detected by SEM. For 5 wt% PVA, some beads were also detected. When the content of PVA was increased from 5 wt% to 7 wt%, diameters of the fibers were also increased and the beads were no longer detected. This implies that the electrospun beaded fibers were influenced by the stability of the jet of inorganic material–polymeric solutions, and PVA contents. It should be noted that at low PVA content, the web was composed of fibers and beads. At sufficiently high PVA content, it was exactly right to eject the inorganic material–polymeric solution through the syringe out of the long hollow needle [21], and the product was composed of the bead-free fibers. The diameters of the fibers of Fig. 3b were in the range of 100–250 nm. When they were calcined at 400 °C, 500 °C and 600 °C for 3 h as shown in Fig. 3d–f, the fibers became thinner with their surfaces roughened. These were caused by the evaporation of PVA and volatile components. The nuclei grew up, due to the high temperature calcination indicating that these products were composed of a number of solid nanoparticles joined together in lines shaped like fibers. Upon increasing the calcination temperature, the evaporation rate of PVA and the crystalline degree of inorganic material became higher. At 600 °C, PVA was completely decomposed, and the polycrystalline fibers were produced. At this stage, the diameters of the fibers were in the range of 50–100 nm. The nanoparticles grew up to be larger particles with the average diameter of 100 nm.

Typical TEM and HRTEM images of electrospun fibers after calcination at 500 °C and 600 °C for 3 h are shown in Fig. 4a–c. The results confirmed that the fibers with 500 °C calcination were composed of a number of nanoparticles with average diameter of 50 nm. The corresponding SAED pattern (Fig. 4d) was indexed [22] and specified as $ZnWO_4$ (JCPDS database no. 15-0774) [11]. The (1 3 0) lattice planes (Fig. 4b) were also detected as clear and coherent parallel stripes, composing the crystalline structured $ZnWO_4$. The analysis implies that each of the nanoparticles is single crystal. Upon increasing the calcination temperature from 500 °C to 600 °C, the average size of crystalline particles was increased by 1.5 times of the precursor or about 75 nm in diameter joined together to form fiber-like assembly. Fig. 4e and f shows SAED and simulated patterns of its single crystal. This SAED pattern was indexed [22] and specified as $ZnWO_4$ (JCPDS database no. 15-0774) [11]. It was also in

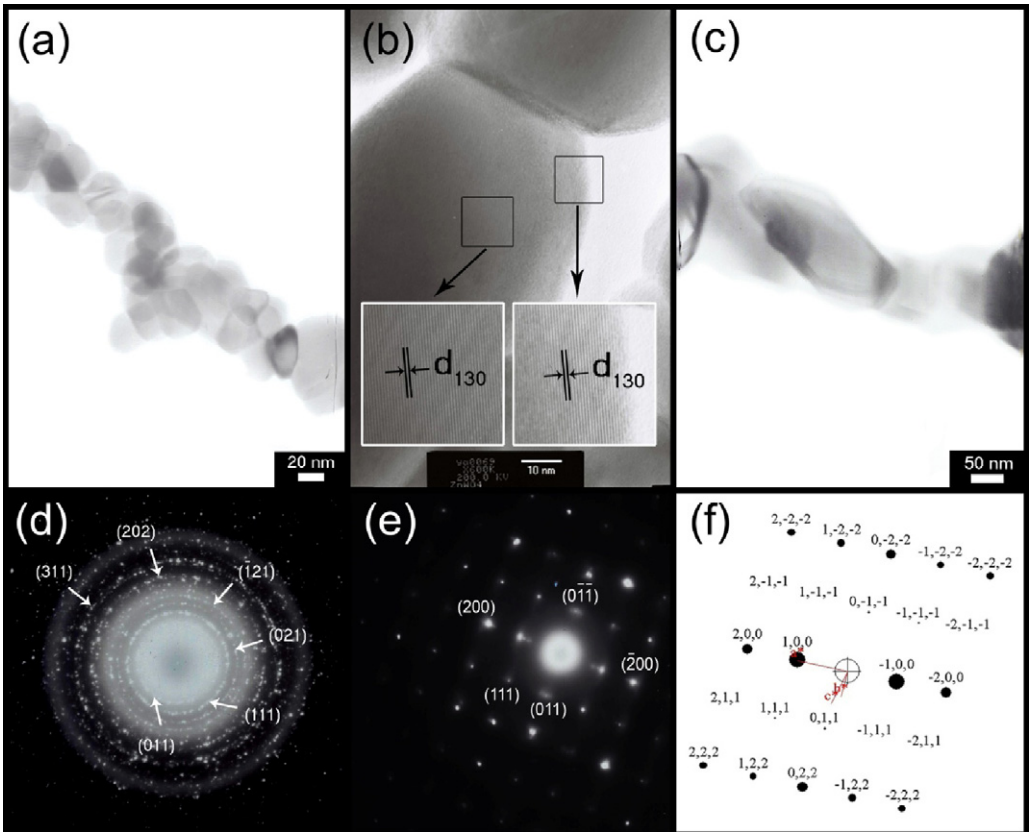

Fig. 4. TEM and HRTEM images, and SAED and simulated patterns of the electrospun fibers after calcination at (a, b and d) 500 °C, and (c, e and f) 600 °C for 3 h.

accordance with that obtained by the simulation [23]. This product was really proved to be monoclinic sanmartinite-type structured $ZnWO_4$.

External morphologies of the electrospun fibers with their corresponding height profiles before (A), and after (B and C) calcination at 500 °C are shown in Fig. 5. In the present research, the as-spun fiber appeared as smooth and even surface, with 250 nm diameter. After calcination at 500 °C, the fiber became thinner. Its surface was roughened and uneven. This product contained different sized particles, connected as fiber-like assembly in accordance with the above SEM and TEM analyses.

3.4. FTIR

To explain the structure of the products in more detail, they were characterized by FTIR in the range between 4000 and 400 cm^{-1}. The FTIR spectra (Fig. 6) were provided further insight into the structure of PVA (*MW* = 125,000), and $ZnWO_4$–PVA electrospun fibers with and without calcination at 400 °C, 500 °C and 600 °C. Obviously, the major vibrational modes associated with poly (vinyl alcohol) were the following. The O—H stretching of alcohol and residual water was detected at 3600–3200 cm^{-1}. The vibrational mode at 2943 cm^{-1} corresponds to the C—H stretching of alkyl groups. The C=O stretching mode was detected at 1721 cm^{-1}, CH_2 bending mode at 1448 cm^{-1}, and C—O stretching mode of carboxyl at 1098 cm^{-1} [24,25]. When the $ZnWO_4$–PVA as-spun fibers were characterized by FTIR, additional six modes were detected at 1000–450 cm^{-1}. They were the stretching and bending modes of Zn—O—W (880, 826 cm^{-1}), W—O in $(WO_6)^{2-}$ octahedrons (709, 660 cm^{-1}), and Zn—O (540, 475 cm^{-1}), respectively [10,17]. Once, the $ZnWO_4$–PVA electrospun fibers were calcined at high temperature, the PVA began to evaporate and decompose. At higher temperatures, the evaporation rates were faster and the PVA spectra became lessened. Until at 600 °C calcination, the vibrational modes of PVA were no longer detected, and those of $ZnWO_4$ were the strongest.

3.5. Raman analysis

The Raman spectra of $ZnWO_4$–PVA electrospun fibers with 400 °C, 500 °C, and 600 °C calcination are shown in Fig. 7. It should be noted that the Raman peaks of the electrospun fibers with 400 °C calcination were broadened, caused by the dispersion of the crystallite sizes and relaxation of the $ZnWO_4$ particles [7]. When the calcination temperatures were increased to be 500 °C and 600 °C, the $ZnWO_4$ crystals were improved and its crystalline degree was increased. These promoted the atoms to concurrently vibrate at the same mode and the intensity increased in the strength. The spectra show the peaks at 195 cm^{-1} which was interpreted as $\nu(A_g)$ involving the Zn^{2+} cations. The peaks at 277 cm^{-1} were specified as $\nu_{def}(A_g)$ of the cationic sublattices. Those at 344 and 409 cm^{-1} were assigned as $r(B_g)$ and $\delta(A_g)$ deformation modes, and at 783 cm^{-1} and 901 cm^{-1} as antisymmetric B_g and symmetric A_g modes of the terminal WO_2 groups, including at 515 and 547 cm^{-1} as $\nu_{sym}(B_g)$ and $\nu_{sym}(A_g)$, and at 678 and 710 cm^{-1} as $\nu_{as}(A_g)$ and $\nu_{as}(B_g)$ modes of the $(W_2O_4)_n$ chains, reported by Kloprogge et al. [16], respectively. These last two vibrations were reported as B_g and A_g internal stretching modes, reported by Errandonea et al. [26] and Siriwong et al. [27]. The Raman spectra were also used to prove the crystalline $ZnWO_4$.

3.6. Formation mechanism

A possible formation mechanism of $ZnWO_4$–PVA electrospun fibers produced by electrospinning was proposed according to the above results as follows. The mixture solution of zinc acetate dihy-

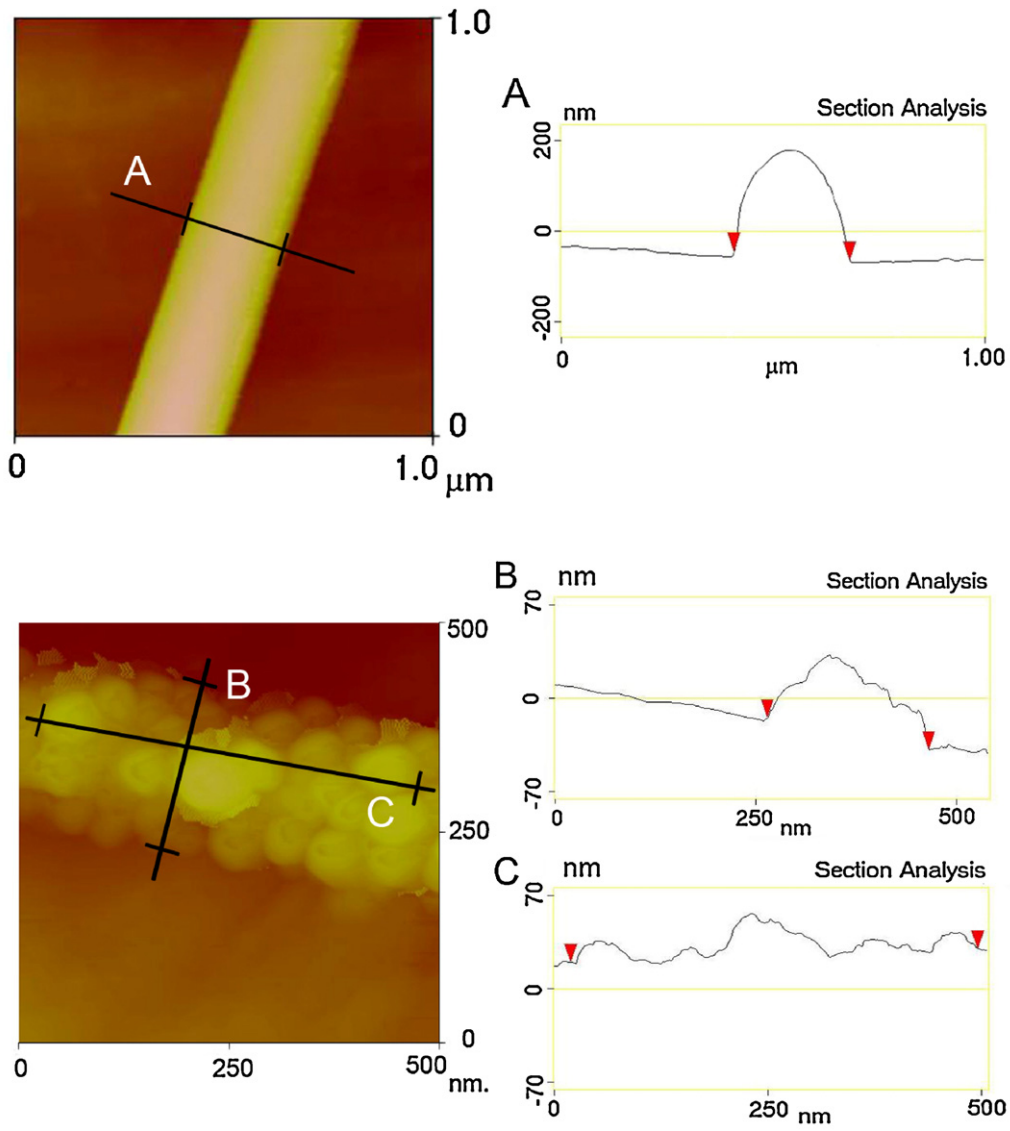

Fig. 5. AFM images and height profiles of the electrospun fibers before (A), and after (B and C) calcination at 500 °C for 3 h.

drate, ammonium metatungstate hydrate and PVA was ejected out of a hollow needle as a non-woven fiber. Concurrently, a high direct voltage was supplied to the needle tip. The external electric field (**E**) developed inside the fiber, axially pointed towards the grounded collector. Thus the fiber was heated up. Zinc acetate dihydrate reacted with ammonium metatungstate hydrate to produce $ZnWO_4$ molecules, which nucleated and blended in PVA template.

$$12Zn(CH_3COO)_2 \cdot 2H_2O + H_{26}N_6O_{40}W_{12} \cdot H_2O + 31H_2O \rightarrow 12ZnWO_4 + 48CO_2 + 105H_2 + 3N_2 \quad (1)$$

At this stage, $ZnWO_4$–PVA electrospun product shaped like fibers formed and deposited as a web of fibers on a grounded aluminum foil (Figs. 3a–c, and 5 (left top)). Upon calcination at 400–600 °C, PVA and residual water evaporated and decomposed. $ZnWO_4$ nuclei grew to form nanoparticles (Figs. 3d–f, 4a–c, and 5 (left bottom)). The rates of evaporation and decomposition increased with the increasing in the calcination temperature. At 600 °C, PVA and water were no longer detected (Figs. 1, 4e and 6e). A number of the nanoparticles joined together in line shaped like a web of nanofibers.

3.7. UV–visible absorption

UV–visible absorption of $ZnWO_4$–PVA electrospun fibers after calcination at 600 °C is shown in Fig. 8, which indicated an exponential decreasing of the photonic absorbance attenuated through the material. For crystalline semiconductors, the UV absorption near band edge follows the equation.

$$\alpha h\nu = (h\nu - E_g)^n \quad (2)$$

where α, h, ν, and E_g are the absorbance, Planck constant, photon frequency, and photonic energy band gap, respectively. The parameter n is a pure number associated with the different types of electronic transitions: $n = 1/2$, 2, 3/2 or 3 for direct-allowed, indirect-allowed, direct-forbidden and indirect-forbidden transitions, respectively [10,15,28,29]. It should be noted that the absorption was controlled by two photon energy ($h\nu$) ranges – the high and low energies. When the photon energy is greater than the energy band gap (E_g), absorption is linearly increased with the increasing of photon energy. The steep inclination of the linear portion of the curve was caused by the UV absorption for charged transition from the topmost occupied state of valence band to the bottommost unoccupied state of the conduction band. For the pho-

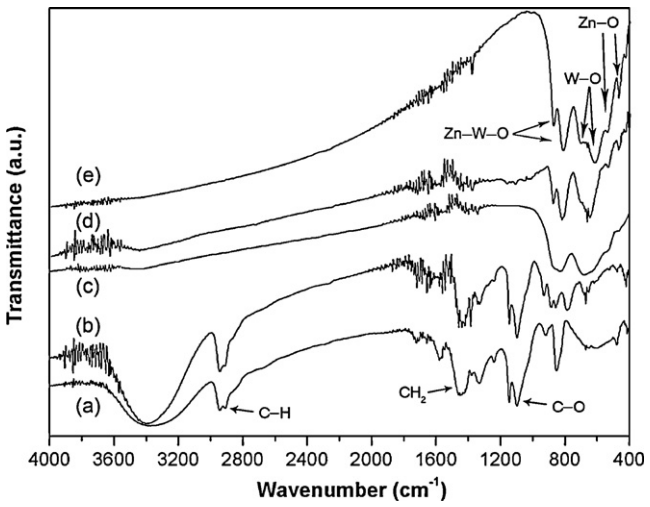

Fig. 6. FTIR spectra of (a) PVA, and (b–e) $ZnWO_4$–PVA electrospun fibers before and after calcination at 400 °C, 500 °C, and 600 °C for 3 h, respectively.

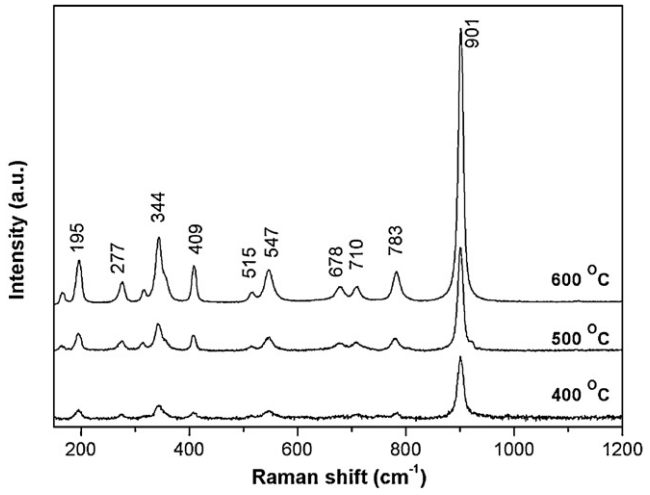

Fig. 7. Raman spectra of $ZnWO_4$–PVA electrospun fibers after calcination at 400 °C, 500 °C, and 600 °C for 3 h.

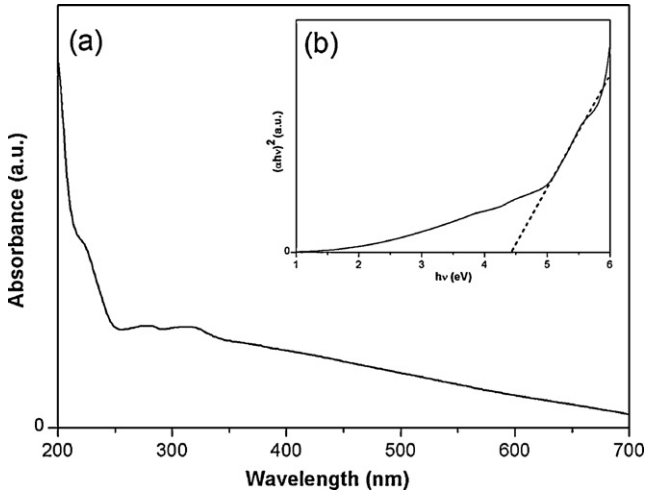

Fig. 8. UV–visible absorption of $ZnWO_4$–PVA electrospun fibers after calcination at 600 °C for 3 h.

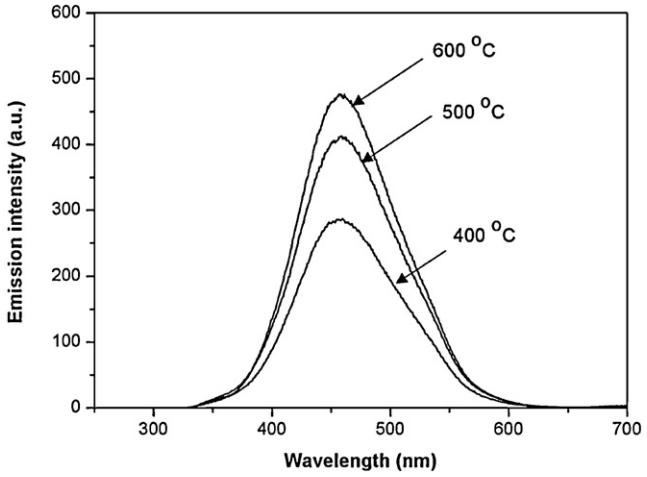

Fig. 9. PL emission of $ZnWO_4$–PVA electrospun fibers after calcination at 400 °C, 500 °C, and 600 °C for 3 h.

ton energy with less than E_g, the absorption curve became different from linearity, which was caused by the UV absorption for charged transition relating to defect levels. Its direct energy gap was determined by extrapolating the linear portion curve of the $(\alpha h\nu)^2$ vs $h\nu$ plot to $\alpha = 0$ (zero absorption). For the present work, direct energy gap was 4.42 eV – very close to those of 3.9–4.4 eV reported by Lacomba-Perales et al. [30], and 4.01 eV reported by Zhao et al. [10]. For tungstates, the top occupied states of valence band correspond to O_{2p}, and the lowest unoccupied states of conduction band to W_{5d} [27]. For bivalent metal tungstates, the hybridization of the valence states of the metal with O_{2p} and W_{5d} states played an important role in determining the energy band gap. A wide band gap was achieved for those of the tungstates with the s states of the bivalent cations hybridized with the O_{2p} and W_{5d} states, while a narrow band gap was caused by the p, d, and f states hybridization. As for a wide band gap of $ZnWO_4$, the s states hybridization seemed to be taken into account in the electronic transition. The transition of excitons (electron–hole pairs) between the O_{2p} and W_{5d} orbitals of pure WO_3 was induced by photonic absorption – the O_{2p} orbitals constituted the valence band, and the W_{5d} orbitals the conduction band. For transition metal tungstates – $ZnWO_4$ excluded, the valence orbitals of the transition metal cations ($Co^{II}(3d^7)$, $Ni^{II}(3d^8)$, $Cu^{II}(3d^9)$) hybridized with the W_{5d} orbitals to make the constitution of the conduction band different. For $Zn^{II}(3d^{10})$, the only possibility is to form the conduction band composed of Zn_{3s} and W_{5d} states, in order to enlarge the energy band gap (E_g) [28]. However, particle-sizes and morphologies were found to play the role in the absorbance characteristics [15], which have the influence on the energy gap as well.

3.8. PL emission

The optical property of $ZnWO_4$ nanofibers with calcination at high temperatures was studied using 280 nm excitation wavelength, and the results are shown in Fig. 9. In this research, the emission peaks presented broad bands over the 350–600 nm range with a strong blue emission peaks centered at the same wavelengths of 460 nm in accordance with the report of Chen et al. [31]. The transitions were caused by the hybridization of the W_{5d} and O_{2p} states with very strong tendency for self-trapping of the $(WO_6)^{2-}$ octahedral structure of $ZnWO_4$, in response to this PL emission [15]. The luminescence intensity was increased with the increasing of the calcination temperature, in accordance with the improvement of crystalline degree characterized by the above XRD analysis.

4. Conclusions

A solution of zinc acetate dihydrate and ammonium metatungstate hydrate with 1:1 molar ratio of Zn:W was prepared and further mixed with 5 wt%, 6 wt%, and 7 wt% PVA, to form three mixtures. By using the +15 kV direct voltage, these mixtures were electrospun to form the webs of $ZnWO_4$–PVA fibers on the ground aluminum foils. In the present research, the electrospun fibers of 6 wt% PVA were further calcined at 400–600 °C for 3 h to form $ZnWO_4$ nanofibers. At 600 °C, the product was $ZnWO_4$ nanoparticles joined together in line shaped like a web of spiders with their direct energy gap of 4.42 eV caused by the hybridization of Zn_{3s} and W_{5d} states, and luminescence at 460 nm (blue) by the transition of the $(WO_6)^{2-}$ octahedrons – one of the promising materials for a variety of applications.

Acknowledgements

We wish to thank the Thailand's Office of the Higher Education Commission for providing financial support through the National Research University (NRU) Project, and the Thailand Research Fund (TRF) through the TRF Advanced Research Scholar and the Royal Golden Jubilee Ph.D. Program.

References

[1] Z.W. Fu, J. Ma, Q.Z. Qin, Nanostructured $LiCoO_2$ and $LiMn_2O_4$ fibers fabricated by a high frequency electrospinning, Solid State Ionics 176 (2005) 1635–1640.
[2] J.M. Deitzel, J. Kleinmeyer, D. Harris, N.C.B. Tan, The effect of processing variables on the morphology of electrospun nanofibers and textiles, Polymer 42 (2001) 261–272.
[3] J. Lyons, C. Li, F. Ko, Melt-electrospinning part I: processing parameters and geometric properties, Polymer 45 (2004) 7597–7603.
[4] Z.M. Huang, Y.Z. Zhang, M. Kotaki, S. Ramakrishna, A review on polymer nanofibers by electrospinning and their applications in nanocomposites, Compos. Sci. Technol. 63 (2003) 2223–2253.
[5] P.K. Panda, S. Ramakrishna, Electrospinning of alumina nanofibers using different precursors, J. Mater. Sci. 42 (2007) 2189–2193.
[6] J.Y. Li, H. Dai, Q. Li, X.H. Zhong, X.F. Ma, J. Meng, X.Q. Cao, Lanthanum zirconate nanofibers with high sintering-resistance, Mater. Sci. Eng. B 133 (2006) 209–212.
[7] A. Kalinko, A. Kuzmin, Raman and photoluminescence spectroscopy of zinc tungstate powders, J. Lumin. 129 (2009) 1144–1147.
[8] G. Huang, C. Zhang, Y. Zhu, $ZnWO_4$ photocatalyst with high activity for degradation of organic contaminants, J. Alloys Compd. 432 (2007) 269–276.
[9] R.P. Jia, G.X. Zhang, Q.S. Wu, Y.P. Ding, $ZnWO_4$-TiO_2 composite nanofilms: Preparation, morphology, structure and photoluminescent enhancement, Mater. Lett. 61 (2007) 1793–1797.
[10] X. Zhao, W. Yao, Y. Wu, S. Zhang, H. Yang, Y. Zhu, Fabrication and photoelectrochemical properties of porous $ZnWO_4$ film, J. Solid State Chem. 179 (2006) 2562–2570.
[11] Powder Diffract. File, JCPDS-ICDD, 12 Campus Boulevard, Newtown Square, PA 19073-3273, USA, 2001.
[12] A. Kornylo, A. Jankowska-Frydel, B. Kuklinski, M. Grinberg, N. Krutiak, Z. Moroz, M. Pashkowsky, Spectroscopic properties of $ZnWO_4$ single crystal doped with Fe and Li impurities, Radiat. Meas. 38 (2004) 707–710.
[13] H. Fu, J. Lin, L. Zhang, Y. Zhu, Photocatalytic activities of a novel $ZnWO_4$ catalyst prepared by a hydrothermal process, Appl. Catal. A 306 (2006) 58–67.
[14] F.S. Wen, X. Zhao, H. Huo, J.S. Chen, E. Shu-Lin, J.H. Zhang, Hydrothermal synthesis and photoluminescent properties of $ZnWO_4$ and Eu^{3+}-doped $ZnWO_4$, Mater. Lett. 55 (2002) 152–157.
[15] M. Hojamberdiev, G. Zhu, Y. Xu, Template-free synthesis of $ZnWO_4$ powders via hydrothermal process in a wide pH range, Mater. Res. Bull. 45 (2010) 1934–1940.
[16] J.T. Kloprogge, M.L. Weier, L.V. Duong, R.L. Frost, Microwave-assisted synthesis and characterisation of divalent metal tungstate nanocrystalline minerals: ferberite, hübnerite, sanmartinite, scheelite and stolzite, Mater. Chem. Phys. 88 (2004) 438–443.
[17] J.H. Ryu, C.S. Lim, K.H. Auh, Synthesis of $ZnWO_4$ nanocrystalline powders, by the polymerized complex method, Mater. Lett. 57 (2003) 1550–1554.
[18] K. Pal, A.K. Banthia, D.K. Majumdar, Preparation and characterization of polyvinyl alcohol–gelatin hydrogel membranes for biomedical applications, AAPS PharmSciTech 8 (2007), doi:10.1208/pt080121, Art. No. 21.
[19] C. Suryanarayana, M.G. Norton, X-ray Diffraction: A Practical Approach, Plenum Press, New York, 1998.
[20] E.A. El-hefian, M.M. Nasef, A.H. Yahaya, The preparation and characterization of chitosan/poly (vinyl alcohol) blended films, E-J. Chem. 7 (2010) 1212–1219.
[21] B. Ding, H.Y. Kim, S.C. Lee, D.R. Lee, K.J. Choi, Preparation and characterization of nanoscaled poly (vinyl alcohol) fibers via electrospinning, Fibers Polym. 3 (2002) 73–79.
[22] K.W. Andrews, D.J. Dyson, S.R. Keown, Interpretation of Electron Diffraction Patterns, Plenum Press, New York, 1971.
[23] C. Boudias, D. Monceau, CaRIne Crystallography 3.1, DIVERGENT S.A., Centre de Transfert, 60200 Compiègne, France, 1989–1998.
[24] H.S. Mansur, R.L. Oréfice, A.A.P. Mansur, Characterization of poly (vinyl alcohol)/poly (ethylene glycol) hydrogels and PVA-derived hybrids by small-angle X-ray scattering and FTIR spectroscopy, Polymer 45 (2004) 7193–7202.
[25] H.S. Mansur, C.M. Sadahira, A.N. Souza, A.A.P. Mansur, FTIR spectroscopy characterization of poly (vinyl alcohol) hydrogel with different hydrolysis degree and chemically crosslinked with glutaraldehyde, Mater. Sci. Eng. C 28 (2008) 539–548.
[26] D. Errandonea, F.J. Manjón, N. Garro, P. Rodríguez-Hernández, S. Radescu, A. Mujica, A. Muñoz, C.Y. Tu, Combined Raman scattering and ab initio investigation of pressure-induced structural phase transitions in the scintillator $ZnWO_4$, Phys. Rev. B 78 (2008) 054116–54121.
[27] P. Siriwong, T. Thongtem, A. Phuruangrat, S. Thongtem, Hydrothermal synthesis, characterization, and optical properties of wolframite $ZnWO_4$ nanorods, CrystEngComm 13 (2011) 1564–1569.
[28] T Montini, V. Gombac, A. Hameed, L. Felisari, G. Adami, P. Fornasiero, Synthesis, characterization and photocatalytic performance of transition metal tungstates, Chem. Phys. Lett. 498 (2010) 113–119.
[29] O. Yayapao, T. Thongtem, A. Phuruangrat, S. Thongtem, CTAB-assisted hydrothermal synthesis of tungsten oxide microflowers, J. Alloys Compd. 509 (2011) 2294–2299.
[30] R. Lacomba-Perales, J. Ruiz-Fuertes, D. Errandonea, D. Martínez-García, A. Segura, Optical absorption of divalent metal tungstates: correlation between the band-gap energy and the cation ionic radius, Europhys. Lett. 83 (2008), doi:10.1209/0295-5075/83/37002, Art. No. 37002.
[31] S.J. Chen, J.H. Zhou, X.T. Chen, J. Li, L.H. Li, J.M. Hong, Z. Xue, X.Z. You, Fabrication of nanocrystalline $ZnWO_4$ with different morphologies and sizes via hydrothermal route, Chem. Phys. Lett. 375 (2003) 185–190.